Neurochemistry International 126 (2019) 19–26

Contents lists available at ScienceDirect

Neurochemistry International

journal homepage: www.elsevier.com/locate/neuint

Virtual screening identification of novel chemical inhibitors for aberrant interactions between pathogenic mutant SOD1 and tubulin

Kazunori Hirayama[a], Yuuki Fujiwara[b], Tohru Terada[c], Kentaro Shimizu[a], Keiji Wada[b], Tomohiro Kabuta[b,*]

[a] Department of Biotechnology, Graduate School of Agricultural and Life Sciences, The University of Tokyo, 1-1-1 Yayoi, Bunkyo-ku, Tokyo, 113-8657, Japan
[b] Department of Degenerative Neurological Diseases, National Institute of Neuroscience, National Center of Neurology and Psychiatry, 4-1-1 Ogawa-Higashi, Kodaira, Tokyo, 187-8502, Japan
[c] Interfaculty Initiative in Information Studies, The University of Tokyo, 7-3-1 Hongo, Bunkyo-ku, Tokyo, 113-0033, Japan

ARTICLE INFO

Keywords:
Virtual screening
ALS
Mutant SOD1
Tubulin
Protein–protein interaction

ABSTRACT

Amyotrophic lateral sclerosis (ALS) is a lethal neurodegenerative disease caused by selective motor neuron death. Mutations in the gene encoding copper/zinc superoxide dismutase (SOD1) belong to one of the four major mutation clusters responsible for pathogenesis of ALS. Toxic gain-of-function (not loss-of-function) of SOD1 mutants causes motor neuron degeneration. Aberrant protein–protein interactions (PPI) between mutant SOD1 and other proteins are involved in this toxic gain-of-function. Therefore, PPI inhibitors of mutant SOD1 not only increase understanding of ALS pathogenesis, but can also be used as novel therapeutics for ALS. Although it is challenging to identify PPI inhibitors, prior knowledge of the binding site can increase success probability. We have previously reported that tubulin interacts with N-terminal residues 1–23 of mutant SOD1. In the present study, we performed virtual screening by docking simulation of 32,791 compounds using this N-terminal binding site as prior knowledge. An established assay system for interaction inhibition between mutant SOD1–tubulin was used as an in-house model system to identify mutant SOD1 PPI inhibitors, with the goal of developing novel therapeutics for ALS. Consequently, five of six assay-executable compounds among top-ranked compounds during docking simulation inhibited the mutant SOD1–tubulin interaction *in vitro*. Binding mode analysis predicted that some inhibitors might bind the tubulin binding site of G85R SOD1 by pi electron interaction with the aromatic ring of the Trp32 residue of G85R SOD1. Our screening methods may contribute to the identification of lead compounds for treating ALS.

1. Introduction

Amyotrophic lateral sclerosis (ALS) is a lethal neurodegenerative disease caused by selective motor neuron death. Occurrence of ALS is approximately 2 per 100,000 people per year, with a slightly higher ratio in males. Most ALS is sporadic (SALS), with 5%–10% regarded as familial (FALS) (Byrne et al., 2012). However, the incidence of FALS is likely to be underestimated because of ambiguity on whether ALS is sporadic or familial (Al-Chalabi and Lewis, 2011). More than 100 genes are reported to be relevant to FALS, with 20 causative genes identified (OMIM). Of these 20 genes, four major genes have been identified: copper/zinc superoxide dismutase (SOD1), TAR DNA-binding protein 43 (TARDBP)/TDP-43, C9orf72, and fused in sarcoma (FUS) (Alsultan et al., 2016; Morgan et al., 2017). SOD1 mutation is responsible for 20% of FALS and 2%–7% of sporadic cases (ALSOD: http://alsod.iop.kcl.ac.uk/Overview/gene.aspx?gene_id=SOD1). The number of reported SOD1 mutations derived from ALS patients is 185 (ALSOD, accessed on Aug. 2018). Mutant SOD1 causes motor neuron death by gain-of-toxicity and not loss-of-function (Gurney et al., 1994; Reaume et al., 1996). Aberrant protein–protein interactions (PPI) between mutant SOD1 and other proteins are involved in this toxic gain-of-function (Ilieva et al., 2009). Although the mechanism underlying FALS has been elucidated to a certain degree, no consensus or detailed mechanism of SALS pathogenesis has been identified (Ilieva et al., 2009). Because of its complex pathogenesis, there are currently no approved SOD1 inhibitors as ALS therapeutics (Dervishi and Ozdinler, 2018). SOD1 and its mutants are important targets, not only for developing novel therapeutics for ALS, but also for identifying PPI inhibitors.

We previously reported that TDP-43, which is associated with FALS, interacts with mutant SOD1 at its dimerization interface (Higashi et al.,

* Corresponding author.
E-mail address: kabuta@ncnp.go.jp (T. Kabuta).

https://doi.org/10.1016/j.neuint.2019.02.020
Received 12 October 2018; Received in revised form 22 January 2019; Accepted 25 February 2019
Available online 01 March 2019
0197-0186/

Abbreviations

ADME/Tox	absorption, distribution, metabolism, excretion and toxicity
ALS	Amyotrophic lateral sclerosis
ALSOD	A user-friendly online bioinformatics tool for amyotrophic lateral sclerosis genetics
FALS	familial ALS
FDA	Food and Drug Administration
FUS	fused in sarcoma
GFP	green fluorescent protein
IL	interleukin
KIFAP3	kinesin-associated protein 3
MDM2	mouse double minute 2
MIF	macrophage migration inhibitory factor
PBS	phosphate-buffered saline
PDB	Protein Data Bank
PPI	protein-protein interaction
RMSD	root mean square deviation
SALS	sporadic ALS
SBDD	structure-based drug design
SNAP25	synaptosomal associated protein 25
SOD1	copper/zinc superoxide dismutase
TARDBP	TAR DNA-binding protein 43
UCH-L1	ubiquitin carboxyl-terminal hydrolase isozyme L1
UCH-L3	ubiquitin carboxyl-terminal hydrolase isozyme L3

2010). Meanwhile, another group reported that mutant SOD1 specifically associates with Derlin-1, causing gain-of-toxicity and inducing motor neuron-specific cell death via endoplasmic reticulum stress. Moreover, this toxicity is likely obtained through direct interaction with Derlin-1 (Nishitoh et al., 2008). Corroboratively, most ALS-linked SOD1 mutations are also Derlin-1 interacting mutations (Fujisawa et al., 2015). Recently, the same group also reported that inhibiting the interaction between mutant SOD1 and Derlin-1 can lead to amelioration of ALS symptoms in model mice (Tsuburaya et al., 2018). Nonetheless, despite these studies, further study on how mutant SOD1 affects ALS is still needed, especially for SALS, as well as detailed pathophysiology of PPI with other proteins. Studies have implicated PPI with mutant SOD1 aside from Derlin-1, therefore a novel interaction of mutant SOD1 may be involved in pathogenesis of ALS. Indeed, interaction between misfolded mutant SOD1 and kinesin-associated protein 3 (KIFAP3), a subunit of kinesin-2 motor protein (Tateno et al., 2009), and various synapse-related molecules, such as synaptotagmin and synaptosomal associated protein 25 (SNAP25) have already reported in FALS patient tissue (Araki et al., 2012). Recently, an interaction was reported between G85R SOD1 and N110C mutant of macrophage migration inhibitory factor (MIF) (Shvil et al., 2018). Further, we have shown that mutant SOD1 interacts with tubulin and affects tubulin polymerization (Kabuta et al., 2009). We have also shown that mutant SOD1 interacts with tubulin via the N-terminal residues 1–23 of SOD1 (Kabuta et al., 2009), which are adjacent to the SOD1–Derlin-1 binding site (N-terminal residues 5–18 of SOD1). Here, we aimed to identify PPI inhibitors of mutant SOD1 as ALS therapeutics, taking advantage of the known tubulin binding site of mutant SOD1 and the interaction as a test case. Furthermore, as the crystal structure of mutant SOD1 is available, we determined the applicability of structure-based drug design (SBDD) for the purpose of identifying PPI inhibitors.

SBDD is used to discover novel inhibitors for PPI as it enables rapid and economical hit identification compared with classical screening methods for *in vitro* or *in vivo* biological assays. *In silico* drug screening approaches, such as molecular docking, offer a shortcut when the crystal structure of at least one target protein is available for PPI.

Docking simulation has widely been used for screening of enzyme inhibitors (McNally et al., 2003; Peng et al., 2003), and a rational design of SOD1 enzymatic inhibitors by combining copper chelating and coordinating fragments has also been reported (Dong et al., 2016). Recently, docking simulation was used for virtual screening, with successful identification of several PPI inhibitors. Small molecule inhibitors for the interleukin (IL)-15/IL-15R interaction that are active in cells were identified in combination with chemical synthesis of lead compounds (Quemener et al., 2017). Moreover, five compounds targeting the PPI interface between Menin–Mixed Lineage Leukemia with novel scaffolds were also identified (Xu et al., 2016). In addition, four inhibitors for the mouse double minute 2 (MDM2)–p53 interaction were identified in combination with X-ray co-crystallization (Tortorella et al., 2016). All of these three approaches share both pharmacophore-based and docking-based virtual screening.

SBDD has also been used to find inhibitors of protein aggregation. Most of the ALS-associated mutations in SOD1 increase the aggregation propensity of the protein (Prudencio et al., 2009). Several studies regarding inhibition of SOD1 aggregation were reported (Banerjee et al., 2017; Ray et al., 2005).

However, correct prediction of PPI sites is still a major hindrance for identifying PPI inhibitors. It is difficult to resolve PPI at atomic resolution by *in silico* methods, although it may not be necessary for identification of PPI inhibitors. Accordingly, an approach where docking simulation is performed against an experimentally-determined PPI site is promising. Using this approach, conventional protein–ligand docking simulation for identification of PPI inhibitors can be performed. Thus, rather than depending on *in silico* tools only, *in vitro* experimental results can be used as input for *in silico* tools, such as interaction site information. Thereby, reasonable results can be acquired from *in silico* tools.

Among many docking simulation platforms, we use GOLD. Many successful cases of predicting binding modes of lead compounds or identifying protein ligand inhibitors have been reported with GOLD

Table 1
List of top-ranked 11 compounds identified by virtual screening according to GOLD score.

No.	Compound name	Mol. Weight	GOLD score
1	N-(3-chlorophenyl)-2-[(2,5-dioxo-1-phenyl-3-pyrrolidinyl)thio]acetamide	375	53.06
2	N-[(2-hydroxy-8-methyl-3-quinolinyl)methyl]−N-(2-methoxyethyl)benzamide	350	52.18
3	2-[(5-butyl-4-methyl-4H-1,2,4-triazol-3-yl)thio]−N-(3-methylphenyl)acetamide	318	51.27
4	N-(3-chloro-2-methylphenyl)-2-{[1-(4-oxo-3,4-dihydro-2-quinazolinyl)ethyl]thio}acetamide	388	53.14
5	N-(2-ethoxyphenyl)-3-[3-(2-ethoxyphenyl)-1,2,4-oxadiazol-5-yl]propanamide	381	52.27
6	3-[3-(2-ethoxyphenyl)-1,2,4-oxadiazol-5-yl]−N-(4-methylphenyl)propanamide	351	51.96
7	N-(2,4-dimethylphenyl)-3-[3-(2-ethoxyphenyl)-1,2,4-oxadiazol-5-yl]propanamide	365	52.24
8	N-{[benzyl(2-furylmethyl)amino]carbonyl}-4-methylbenzenesulfonamide	384	53.37
9	N-isopropyl-4-methoxy-N-[(3-phenyl-1,2,4-oxadiazol-5-yl)methyl]benzamide	351	52.42
10	N-(2-ethoxyphenyl)-2-{[4-ethyl-5-(2-furyl)-4H-1,2,4-triazol-3-yl]thio}acetamide	372	52.08
11	N-(2-ethoxyphenyl)-2-{[4-methyl-5-(4-methylphenyl)-4H-1,2,4-triazol-3-yl]thio}acetamide	383	51.47

Table 2
List of assay-executable six compounds and their inhibitory effects on the tubulin–G85R SOD1 interaction.

No.	Compound name	% inhibition
1	N-(3-chlorophenyl)-2-[(2,5-dioxo-1-phenyl-3-pyrrolidinyl)thio]acetamide	96.6
2	N-[(2-hydroxy-8-methyl-3-quinolinyl)methyl]−N-(2-methoxyethyl)benzamide	0
3	2-[(5-butyl-4-methyl-4H-1,2,4-triazol-3-yl)thio]−N-(3-methylphenyl)acetamide	38.6
8	N-{[benzyl(2-furylmethyl)amino]carbonyl}-4-methylbenzenesulfonamide	48.2
9	N-isopropyl-4-methoxy-N-[(3-phenyl-1,2,4-oxadiazol-5-yl)methyl]benzamide	96.3
10	N-(2-ethoxyphenyl)-2-{[4-ethyl-5-(2-furyl)-4H-1,2,4-triazol-3-yl]thio}acetamide	46.4

Band intensities of western blotting were converted to tubulin–G85R SOD1 interaction inhibition rate by the following equation: (sample intensity without compound) − (sample intensity with tested compound)/(sample intensity without compound) − (sample intensity with tubulin and without SOD1). Tested assay-executable compounds were as follows: compound **1, 2**, **3**, **8, 9,** and **10** (concentration of all compounds is 200 μM).

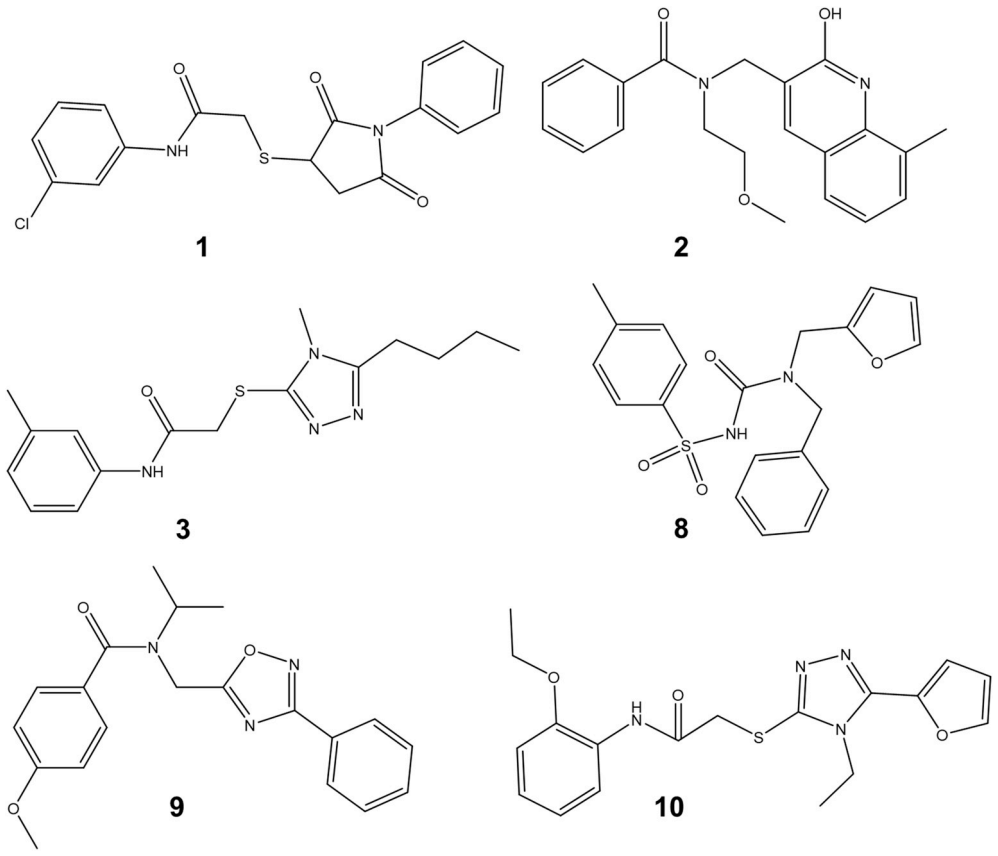

Fig. 1. Chemical structures of assay-executable six compounds among the top-11 ranked compounds predicted by GOLD screening.

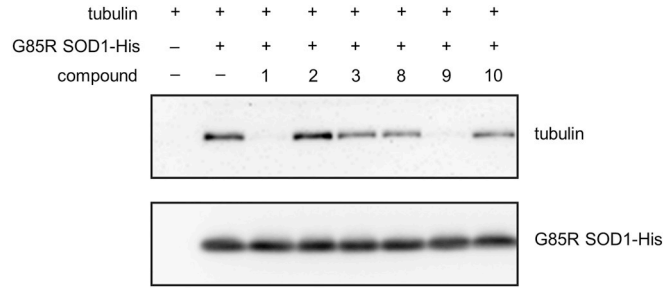

Fig. 2. Pull-down assay results showing inhibitory effects of assay-executable compounds on the tubulin–G85R SOD1 interaction. Western blotting was performed using recombinant His-tagged G85R SOD1, tubulin, and each compound.

(Karatas et al., 2017; Lagarias et al., 2018; Oyallon et al., 2018; Ramsbeck et al., 2018). Among them, some groups have reported successful identification of PPI inhibitors with GOLD (Villa et al., 2018; Zhou et al., 2018).

In this study, docking simulation against the G85R SOD1–tubulin binding site was examined by pull-down assay to validate efficacy of this SBDD method. Altogether, we identified five inhibitors (inhibition rate = 38.6%–96.6%) of the G85R SOD1–tubulin interaction by GOLD virtual screening of 32,791 compounds.

2. Material and methods

2.1. Compound library

The ADME/Tox (absorption, distribution, metabolism, excretion and toxicity) filtered virtual compound library was used, which consists of 32,791 chemical compounds (all from ChemBridge CNS-Set, designed to penetrate the blood–brain barrier; ChemBridge Corporation,

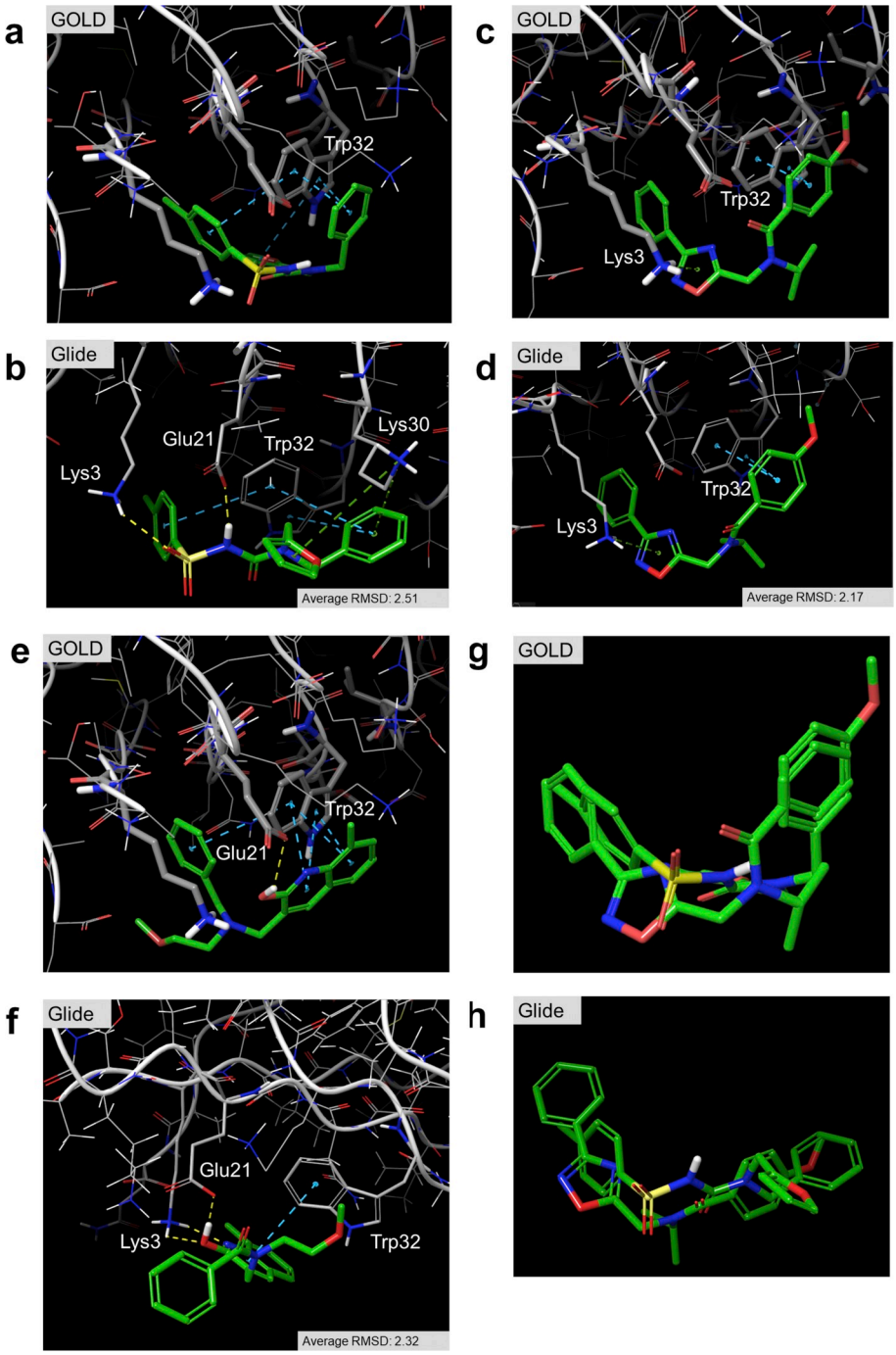

Fig. 3. Schematic showing molecular docking results of the tested compounds. (a–f) Binding modes of compound **8** (a, b), compound **9** (c, d), and compound **2** (e, f) are shown with the interacting residues of SOD1. For Glide results, RMSDs from the top-ranked pose were calculated for all but the top-ranked pose. The average value is shown in right bottom of each figure. The hydrogen bond is depicted as a yellow dashed line. Pi–pi electron stacking interactions are depicted as blue dashed lines, with the pi electron–cation interaction depicted as a green dashed line. Oxygen atoms are shown in red, nitrogen atoms in blue, a sulfur atom in yellow, and polar hydrogen atoms in white. Carbons of G85R SOD1 are shown in light grey and those of the compounds in green. (g, h) Superposition of the docking poses of compounds **8** and **9** generated by GOLD (g) and Glide (h). The figures were prepared using Maestro (Schrödinger, LLC, New York, NY, USA).

San Diego, CA, USA) (conformation acquired from Ressource Parisienne en BioInformatique Structurale site, accessed in 2007).

2.2. Protein data preparation

Human G85R SOD1 crystal structure data (PDB code; 2VR6) were obtained from the Protein Data Bank (PDB) (https://www.rcsb.org/). Hydrogens were added to G85R SOD1 and energy minimized using Chimera 1.3 (Pettersen et al., 2004), with all heavy atoms fixed.

2.3. Virtual screening

Virtual screening experiments were performed using GOLD 4 (Cambridge Crystallographic Data Centre [CCDC], Cambridge, UK) (Jones et al., 1997). Compounds were screened with automatic genetic algorithm parameter settings to maximize efficiency in terms of calculation time. The optimal number of operations for each compound was automatically calculated. Protein side chain flexibility was not considered. Solvent-accessible surfaces of the binding site were limited using a cavity detection algorithm (Hendlich et al., 1997). Binding site residues composed of Lys3, Ala4, Val5, Cys6, Ile18, Asn19, Phe20, and Glu21 were specified based on experimentally-determined tubulin binding sites of mutant SOD1 (Kabuta et al., 2009).

Ten docking solutions for each docked molecule were scored and the top-three saved for post-screening evaluation. Potential hydrogen bonds, van der Waals contacts, and other contacts (such as salt bridges and aromatic pi electron interactions) were identified using Maestro (Schrödinger Release, 2016–1; Maestro, Schrödinger, LLC, New York,

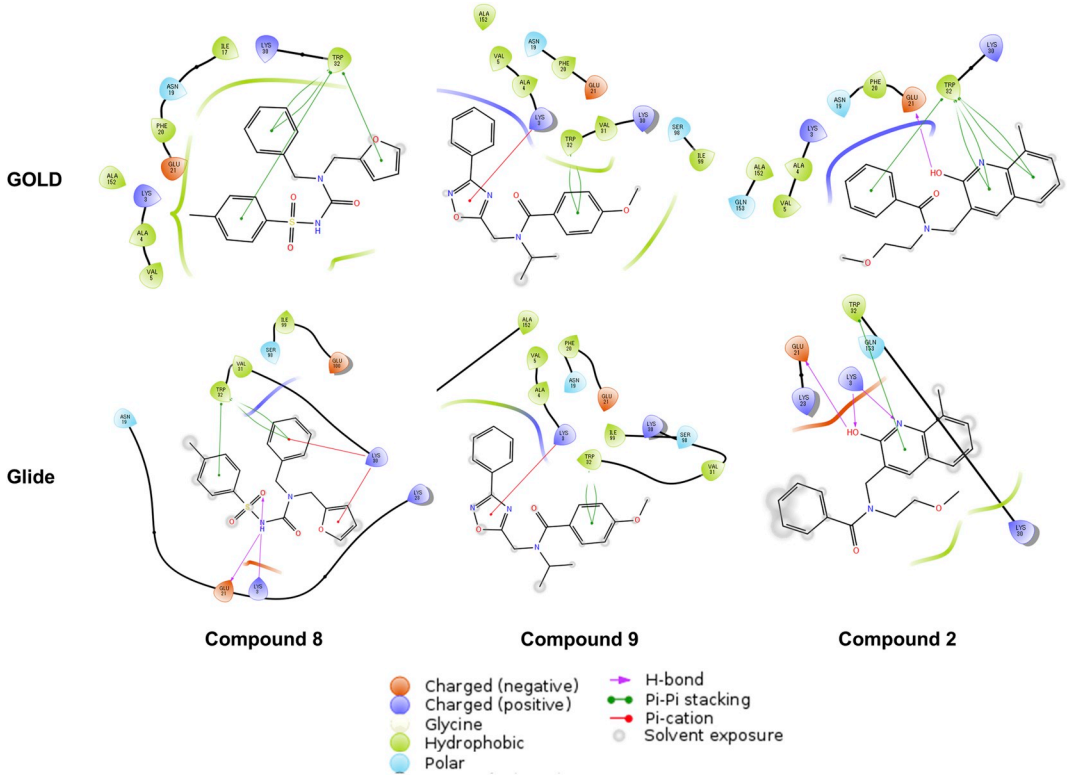

Fig. 4. Protein–ligand interaction diagrams for each compound in the tubulin binding site of G85R SOD1. The diagrams for GOLD and Glide docking results are shown in upper column and lower column, respectively. Teardrop symbols of G85R SOD1 residues are colored by their physicochemical property. The interactions between compounds and G85R SOD1 are depicted by each arrow presented in the caption at the bottom of the figure. The figures were prepared using Maestro (Schrödinger, LLC, New York, NY, USA).

NY, USA). Ligands predicted to be strong-binders by GOLD were used for *in vitro* validation experiments. Virtual screening calculations were performed on 3.16 GHz/Core2Duo CPU personal computers.

2.4. Additional binding mode analysis

Aforementioned human G85R SOD1 (PDB code; 2VR6, chain A) was optimized using protein preparation wizard of Maestro 2017–3 (Schrödinger, LLC, New York, NY, USA) including N-terminal capping.

Three-dimensional conformations of compounds **2**, **8** and **9** were prepared by LigPrep of Maestro 2017-3 (Schrödinger, LLC, New York, NY, USA) based on the SD files provided by the supplier (ChemBridge Corporation) under the basically default condition. For compounds **2** and **8**, LigPrep was run under the condition not changing ionization and not generating tautomers in order to maintain the original chemical structures.

Three compounds **2**, **8** and **9** were docked to the optimized G85R SOD1 using Glide (Schrödinger, LLC, New York, NY, USA) SP mode under condition writing out at most 10 poses per compound. Ligand interaction diagram module of Maestro 2017-3 was utilized for visualizing interactions between a compound and human G85R SOD1 residues.

2.5. Reagents

Human recombinant G85R SOD1 was prepared as described previously (Kabuta et al., 2009). A murine anti-His tag monoclonal antibody, 9C11, and rabbit anti-α-tubulin antibody, 9F3, were purchased from FUJIFILM Wako Pure Chemical Corporation (Doshomachi, Osaka, Japan) and Cell Signaling Technology, Inc. (Danvers, MA, USA), respectively.

Compounds within the ChemBridge CNS-Set (supplier IDs given in parentheses) were as follows: Compound **1**: N-(3-chlorophenyl)-2-[(2,5-dioxo-1-phenyl-3-pyrrolidinyl)thio]acetamide (5211550); Compound **2**: N-[(2-hydroxy-8-methyl-3-quinolinyl)methyl]−N-(2-methoxyethyl)benzamide (9000281); Compound **3**: 2-[(5-butyl-4-methyl-4H-1,2,4-triazol-3-yl)thio]−N-(3-methylphenyl)acetamide (9000414); Compound **4**: N-(3-chloro-2-methylphenyl)-2-{[1-(4-oxo-3,4-dihydro-2-quinazolinyl)ethyl]thio}acetamide (9001952); Compound **5**: N-(2-ethoxyphenyl)-3-[3-(2-ethoxyphenyl)-1,2,4-oxadiazol-5-yl]propanamide (9002439); Compound **6**: 3-[3-(2-ethoxyphenyl)-1,2,4-oxadiazol-5-yl]−N-(4-methylphenyl)propanamide (9003853); Compound **7**: N-(2,4-dimethylphenyl)-3-[3-(2-ethoxyphenyl)-1,2,4-oxadiazol-5-yl]propanamide (9005216); Compound **8**: N-{[benzyl(2-furylmethyl)amino]carbonyl}-4-methylbenzenesulfonamide (9005795); Compound **9**: N-isopropyl-4-methoxy-N-[(3-phenyl-1,2,4-oxadiazol-5-yl)methyl]benzamide (9007144); Compound **10**: N-(2-ethoxyphenyl)-2-{[4-ethyl-5-(2-furyl)-4H-1,2,4-triazol-3-yl]thio}acetamide (9009674); and Compound **11**: N-(2-ethoxyphenyl)-2-{[4-methyl-5-(4-methylphenyl)-4H-1,2,4-triazol-3-yl]thio}acetamide (9010739).

All of these compounds were obtained from ChemBridge Corporation.

2.6. Pull-down assay

Pull-down assay using G85R SOD1 and the 11 compounds was performed as previously reported (Kabuta et al., 2009). Briefly, 15 μg of recombinant His-tagged G85R SOD1, 25 μg of purified tubulin, and 200 μM of each compound were mixed and incubated for 4 h in phosphate-buffered saline (PBS) containing 0.05% Triton X-100. After TALON resin beads were washed three times with PBS containing 0.05% Triton X-100, proteins were eluted using sodium dodecyl sulfate sample buffer.

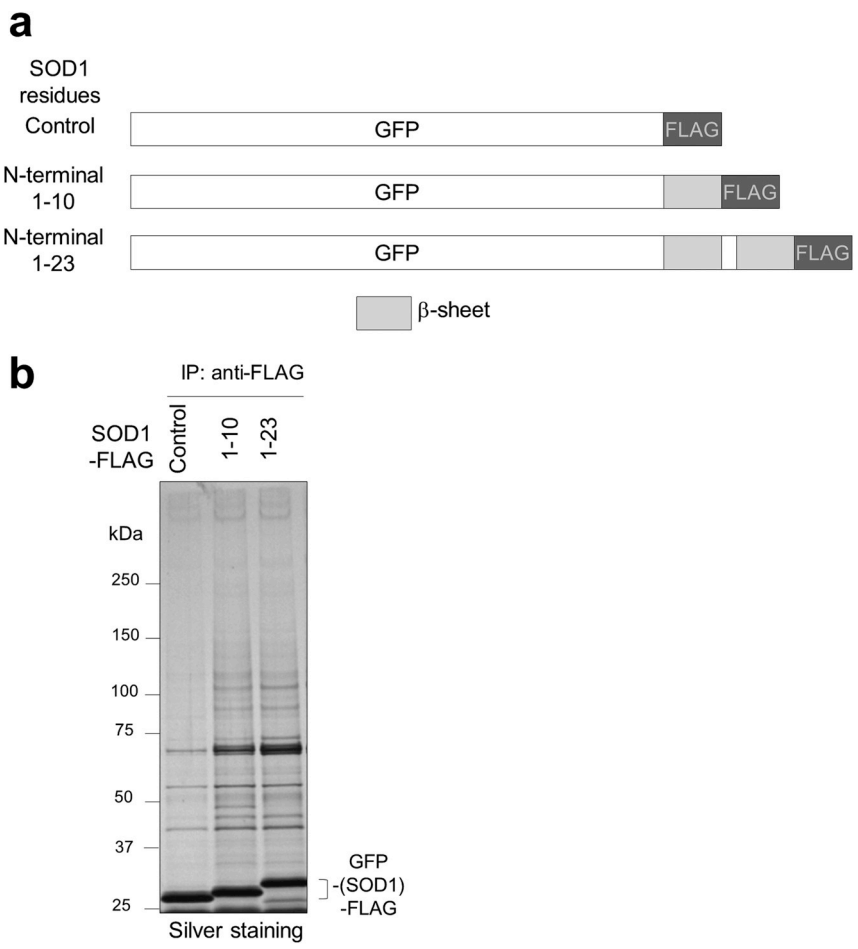

Fig. 5. Immunoprecipitation assay results showing proteins interacting with N-terminal residues (1–10 and 1–23) of SOD1 and FLAG-tagged GFP (green fluorescent protein) as a negative control. (a) Schematic illustration of fusion constructs for the GFP-SOD1 N-terminal region. (b) Lysates of COS-7 cells transfected with the aforementioned constructs were analyzed by immunoprecipitation using an anti-FLAG antibody and silver staining.

2.7. Immunoprecipitation and silver staining

Multiple deletion mutant constructs of FLAG-tagged SOD1 were expressed in COS-7 cells. Cell lysates were then centrifuged and the supernatants immunoprecipitated. Immunoprecipitation was performed by incubating lysates with anti-FLAG M2 affinity gel containing purified immunoglobulin (Millipore–Sigma, Darmstadt, Germany), as previously described (Kabuta et al., 2009). Immunoprecipitated proteins were detected by sodium dodecyl sulfate–polyacrylamide gel electrophoresis followed by silver staining.

3. Results

3.1. Virtual screening

A PDB entry, 2VR6, was used to obtain the three-dimensional structure of G85R SOD1. During virtual screening by GOLD, the protein–ligand interaction site was restricted to the binding site of tubulin (as described in the Material and methods) to ensure that the outcome could be verified by pull-down assay with G85R SOD1–tubulin. Docking simulation by GOLD was performed against 32,791 compounds from CNS-Set, which were pre-filtered by Ressource Parisienne en BioInformatique Structurale under the most modest filtering condition. Overall, 11 compounds with GOLD scores > 50 were predicted to bind to the G85R SOD1 N-terminal region. Specifically, we narrowed down 0.03% of the total number of chemical compounds for validation by pull-down assay (Table 1).

3.2. Inhibitory effect of compounds on mutant SOD1–tubulin interaction

Based on the User Guide for GOLD 3.1, compounds with GOLD scores around 60 may inhibit enzyme activity at half maximal inhibitory concentration (IC_{50}) values of 10–100 μM. Although GOLD scores for the compounds obtained by virtual screening in this study do not meet this criterion, we assumed that relatively low GOLD scores are attributable to the scarcity of cavities on the tubulin binding site of the G85R SOD1 N-terminal region. Therefore, we chose to proceed with our study and validate the top-ranked compounds in terms of GOLD score for identification of PPI inhibitors.

Before performing pull-down assays, compound **4** was found to be insoluble in dimethyl sulfoxide during the preparatory compound solution and aliquot process. Likewise, compounds **5, 6, 7,** and **11** were insoluble in pull-down assay buffer (namely, PBS containing 0.05% Triton X-100). Consequently, we excluded these five compounds (i.e., compounds **4, 5, 6, 7,** and **11**) from the following pull-down assays. Pull-down assays were performed with the remaining six chemicals to determine if they inhibit tubulin–G85R SOD1 binding at the predicted affinities (Table 2, Fig. 1).

Candidate PPI inhibitors predicted by GOLD docking simulation were tested for their ability to inhibit the interaction between tubulin and G85R SOD1. Among these candidates, 5 out of 6 assay-executable compounds inhibited the interaction between tubulin and G85R SOD1. Compounds **1** and **9** strongly inhibited the tubulin interaction of G85R SOD1 (Fig. 2). Compounds **1** and **9** (200 μM) inhibited the interaction by 96.6% and 96.3%, respectively, compared with a negative control

sample with no compound added (Fig. 2, Table 2). Compounds **3, 8,** and **10** partially inhibited the interaction by 38.6%, 48.2%, and 46.4%, respectively. In contrast, with compound **2**, the negative interaction inhibition rate resulted in increased association of tubulin–G85R SOD1, showing that compound **2** was unable to inhibit the interaction between tubulin and G85R SOD1 (Fig. 2, Table 2).

3.3. Predicted binding modes

Predicted binding modes of compounds **8** and **9** to the N-terminal region of G85R SOD1 by GOLD and Glide are shown (Fig. 3a and c: GOLD, Fig. 3b and d: Glide). Although chemical formulae of the two compounds are not similar to each other, predicted docking conformation between these compounds and G85R SOD1 showed similar binding modes. Few hydrogen bonds were observed between the docked ligand and specified binding site (N-terminal region of G85R SOD1) with both compounds **8** and **9** and G85R SOD1 complex structure. Alternatively, several aromatic contacts were observed.

In the biding mode analyzed by GOLD, the aryl group and 4-methylbenzenesulfonamide group of compound **8** appeared to form a pi–pi electron interaction with the aromatic indole ring of Trp32 of G85R SOD1. Meanwhile, the aryl group formed a face-to-face interaction (3.2 Å) with both parts of the indole ring, while the 4-methylbenzenesulfonamide group formed an edge-to-face interaction with the aryl part of the indole ring (4.7 Å). The furyl group of compound **8** appeared to form an edge-to-face pi electron interaction with the pyrrole part of the indole ring of Trp32 (Fig. 3a). A similar docking pose was predicted in the binding mode analysis by Glide, and two hydrogen bonds were predicted between sulfonamide group of compound **8** and Lys3 and Glu21 of G85R SOD1 (Fig. 3b).

In the analysis by GOLD, the phenyl ring of the 4-methoxy-phenyl group of compound **9** appeared to form a face-to-face pi electron interaction with both parts of the indole ring of Trp32. The 1,2,4-oxadiazol ring of compound **9** appeared to form a pi electron–cation interaction with the amino group of Lys3 of G85R SOD1 (Fig. 3c). Docked conformation of compounds **8** and **9** showed similar binding modes on the N-terminal region of G85R SOD1 (Fig. 3g and h), suggesting that the aforementioned pi electron-mediated interactions are essential for inhibitory activity of tubulin–G85R SOD1 interaction. Compound **9** exhibited the same binding mode when docking prediction was performed by Glide (Fig. 3d).

As a non-binder, the predicted docking conformation of compound **2** was analyzed by GOLD. Four face-to-face pi electron interactions and one edge-to-face pi electron interaction were observed between docked compound **2** and the Trp32 residue of G85R SOD1 in the predicted compound **2**/G85R SOD1 complex structure. The quinoline group of compound **2** appeared to form four face-to-face pi electron interactions with the indole group of Trp32, while the aryl group of compound **2** appeared to form an edge-to-face pi electron interaction with the indole group of Trp32. A hydrogen bond between the hydroxyl group of compound **2** and carboxyl group of Glu21 was predicted (Fig. 3e). Relatively similar binding mode was predicted by Glide with only one difference in a hydrogen bond with Lys3 (Fig. 3f).

Although few hydrogen bonds between actual inhibitors (compounds **8** and **9**) and G85R SOD1 were observed, as a non-inhibitor, compound **2** appeared to form a hydrogen bond to SOD1. This hydrogen bond might reflect a bias during docking simulation for compounds to bind stably to the tubulin binding site of G85R SOD1. Schematic diagrams for interaction between each compound and binding site residues of SOD1 are shown in Fig. 4.

We found that various other proteins interact with the N-terminal residues 1–10 or 1–23 of mutant SOD1, shown by immunoprecipitation and silver staining of mutant SOD1–FLAG protein (Fig. 5). Therefore, the PPI inhibitors identified in this study may be useful for analyzing other aberrant interactions with the N-terminal 1–23 residues of mutant SOD1. By elucidating binding sites from deletion mutant experiments, we may be able to identify other PPI inhibitors of mutant SOD1.

4. Discussion

In terms of similarities in chemical features of the identified inhibitors, we were unable to find a common skeleton among them. Instead, we could only extract partial and abstract similarity among them, e.g., a N−C═O group, aromatic ring, and hetero 5-membered ring. Alternatively, there was no hetero 5-membered ring in inactive compound **2**. This is in contrast to ubiquitin carboxyl-terminal hydrolase isozyme L3 (UCH-L3) inhibitors, in which similarity and a common skeleton among them were easily extracted (Hirayama et al., 2007), and likewise with ubiquitin carboxyl-terminal hydrolase isozyme L1 (UCH-L1) potentiators and inhibitors (Mitsui et al., 2010). However, there is conformational similarity among compounds **8** and **9** in terms of aromatic ring disposition in the docked binding mode (Fig. 3d).

Comparing enzymatic inhibitors and PPI inhibitors, there are differences in the degree of pharmacophore similarity despite an almost identical chemical compound library for virtual screening. Regarding enzymatic inhibitors, when target enzymatic proteins have distinct pockets, pharmacophoric features are easily extracted. In contrast, with PPI inhibitors (including the tubulin–mutant SOD1 inhibitors identified in this study), conformational information such as predicted binding mode by docking simulation may aid extraction of a pharmacophore hypothesis. This pharmacophore advantage may be one reason for successful identification of highly active inhibitors in studies showing effective utilization of virtual screening with both docking simulation and pharmacophore modeling (Xu et al., 2016).

Here, we describe approaches to overcome several challenges in identifying PPI inhibitors. First, aromatic stacking is thought to be one of the major components of protein–ligand interactions. Accordingly, compounds that cause the pi electron interaction of Trp32 of G85R SOD1 can bind the N-terminal region of SOD1 with minimally sufficient affinity and inhibit the tubulin interaction (Brylinski, 2018). Second, although aromatic stacking is treated within van der Waals and electrostatic interactions, and no strict calculation of aromatic stacking is performed in docking simulation, aromatic stacking might be better reproduced in docking simulation (Brylinski, 2018). In this study, it is thought that interaction energy calculations, including aromatic stacking by GOLD, effectively worked in predicting inhibitors. Third, the substructure and functional groups of CNS-Set compounds also raises the probability of PPI inhibition. Among the inhibitors identified in this study, compound **1** has a chlorobenzene group that is frequently used in 238 PPI inhibitors as well as Food and Drug Administration (FDA)-approved drugs (Wang et al., 2018).

Finding appropriate binding pockets is essential in PPI inhibitor identification. There is an assumption that the pocket does not change after or during the PPI process. However, this assumption is not accurate because an induced-fit frequently occurs. Therefore, we hypothesize that PPI inhibitors can be identified through normal protein–ligand docking using prior PPI site information for one of the proteins. We believe that this hypothesis is at least useful for identifying PPI inhibitors.

Although high-throughput screening is a major methodology for large numbers of screening compounds, in this study we show that PPI inhibitors can be identified among a relatively small number of compounds in combination with biological validation, namely binding site determination.

Acknowledgments

This work was supported by Grants-in-Aid for Scientific Research from the Japan Society for the Promotion of Science (22790838 to T.K.; 25290027 to K.W.); a research grant from the Takeda Science Foundation (to T.K.); Intramural Research Grants for Neurological and Psychiatric Disorders of NCNP (to T.K.); and a grant from Japan Agency for Medical Research and Development (16ek0109048h to K.W.).

References

Al-Chalabi, A., Lewis, C.M., 2011. Modelling the effects of penetrance and family size on rates of sporadic and familial disease. Hum. Hered. 71, 281–288.

Alsultan, A.A., Waller, R., Heath, P.R., Kirby, J., 2016. The genetics of amyotrophic lateral sclerosis: current insights. Degener. Neurol. Neuromuscul. Dis. 6, 49–64.

Araki, T., Nagano, S., Tateno, M., Kaido, M., Ogata, K., Arima, K., 2012. Misfolded SOD1 forms high-density molecular complexes with synaptic molecules in mutant SOD1-linked familial amyotrophic lateral sclerosis cases. J. Neurol. Sci. 314, 92–96.

Banerjee, V., Oren, O., Ben-Zeev, E., Taube, R., Engel, S., Papo, N., 2017. A computational combinatorial approach identifies a protein inhibitor of superoxide dismutase 1 misfolding, aggregation, and cytotoxicity. J. Biol. Chem. 292, 15777–15788.

Brylinski, M., 2018. Aromatic interactions at the ligand-protein interface: implications for the development of docking scoring functions. Chem. Biol. Drug Des. 91, 380–390.

Byrne, S., Elamin, M., Bede, P., Hardiman, O., 2012. Absence of consensus in diagnostic criteria for familial neurodegenerative diseases. J. Neurol. Neurosurg. Psychiatry 83, 365–367.

Dervishi, I., Ozdinler, P.H., 2018. Incorporating upper motor neuron health in ALS drug discovery. Drug Discov. Today 23, 696–703.

Dong, X., Zhang, Z., Zhao, J., Lei, J., Chen, Y., Li, X., Chen, H., Tian, J., Zhang, D., Liu, C., Liu, C., 2016. The rational design of specific SOD1 inhibitors via copper coordination and their application in ROS signaling research. Chem. Sci. 7, 6251–6262.

Fujisawa, T., Yamaguchi, N., Kadowaki, H., Tsukamoto, Y., Tsuburaya, N., Tsubota, A., Takahashi, H., Naguro, I., Takahashi, Y., Goto, J., Tsuji, S., Nishitoh, H., Homma, K., Ichijo, H., 2015. A systematic immunoprecipitation approach reinforces the concept of common conformational alterations in amyotrophic lateral sclerosis-linked SOD1 mutants. Neurobiol. Dis. 82, 478–486.

Gurney, M.E., Pu, H.F., Chiu, A.Y., Dalcanto, M.C., Polchow, C.Y., Alexander, D.D., Caliendo, J., Hentati, A., Kwon, Y.W., Deng, H.X., Chen, W.J., Zhai, P., Sufit, R.L., Siddique, T., 1994. Motor-neuron degeneration in mice that express a human Cu,Zn superoxide-dismutase mutation. Science 264, 1772–1775.

Hendlich, M., Rippmann, F., Barnickel, G., 1997. LIGSITE: automatic and efficient detection of potential small molecule-binding sites in proteins. J. Mol. Graph. Model. 15, 359–363 389.

Higashi, S., Tsuchiya, Y., Araki, T., Wada, K., Kabuta, T., 2010. TDP-43 physically interacts with amyotrophic lateral sclerosis-linked mutant CuZn superoxide dismutase. Neurochem. Int. 57, 906–913.

Hirayama, K., Aoki, S., Nishikawa, K., Matsumoto, T., Wada, K., 2007. Identification of novel chemical inhibitors for ubiquitin C-terminal hydrolase-L3 by virtual screening. Bioorg. Med. Chem. 15, 6810–6818.

Ilieva, H., Polymenidou, M., Cleveland, D.W., 2009. Non-cell autonomous toxicity in neurodegenerative disorders: ALS and beyond. J. Cell Biol. 187, 761–772.

Jones, G., Willett, P., Glen, R.C., Leach, A.R., Taylor, R., 1997. Development and validation of a genetic algorithm for flexible docking. J. Mol. Biol. 267, 727–748.

Kabuta, T., Kinugawa, A., Tsuchiya, Y., Kabuta, C., Setsuie, R., Tateno, M., Araki, T., Wada, K., 2009. Familial amyotrophic lateral sclerosis-linked mutant SOD1 aberrantly interacts with tubulin. Biochem. Biophys. Res. Commun. 387, 121–126.

Karatas, H., Li, Y., Liu, L., Ji, J., Lee, S., Chen, Y., Yang, J., Huang, L., Bernard, D., Xu, J., Townsend, E.C., Cao, F., Ran, X., Li, X., Wen, B., Sun, D., Stuckey, J.A., Lei, M., Dou, Y., Wang, S., 2017. Discovery of a highly potent, cell-permeable macrocyclic peptidomimetic (MM-589) targeting the WD repeat domain 5 protein (WDR5)-Mixed lineage leukemia (MLL) protein-protein interaction. J. Med. Chem. 60, 4818–4839.

Lagarias, P., Vrontaki, E., Lambrinidis, G., Stamatis, D., Convertino, M., Ortore, G., Mavromoustakos, T., Klotz, K.N., Kolocouris, A., 2018. Discovery of novel adenosine receptor antagonists through a combined structure- and ligand-based approach followed by molecular dynamics investigation of ligand binding mode. J. Chem. Inf. Model. 58, 794–815.

McNally, V.A., Gbaj, A., Douglas, K.T., Stratford, I.J., Jaffar, M., Freeman, S., Bryce, R.A., 2003. Identification of a novel class of inhibitor of human and Escherichia coli thymidine phosphorylase by in silico screening. Bioorg. Med. Chem. Lett 13, 3705–3709.

Mitsui, T., Hirayama, K., Aoki, S., Nishikawa, K., Uchida, K., Matsumoto, T., Kabuta, T., Wada, K., 2010. Identification of a novel chemical potentiator and inhibitors of UCH-L1 by in silico drug screening. Neurochem. Int. 56, 679–686.

Morgan, S., Shatunov, A., Sproviero, W., Jones, A.R., Shoai, M., Hughes, D., Al Khleifat, A., Malaspina, A., Morrison, K.E., Shaw, P.J., Shaw, C.E., Sidle, K., Orrell, R.W., Fratta, P., Hardy, J., Pittman, A., Al-Chalabi, A., 2017. A comprehensive analysis of rare genetic variation in amyotrophic lateral sclerosis in the UK. Brain 140, 1611–1618.

Nishitoh, H., Kadowaki, H., Nagai, A., Maruyama, T., Yokota, T., Fukutomi, H., Noguchi, T., Matsuzawa, A., Takeda, K., Ichijo, H., 2008. ALS-linked mutant SOD1 induces ER stress- and ASK1-dependent motor neuron death by targeting Derlin-1. Genes Dev. 22, 1451–1464.

Oyallon, B., Brachet-Botineau, M., Loge, C., Bonnet, P., Souab, M., Robert, T., Ruchaud, S., Bach, S., Berthelot, P., Gouilleux, F., Viaud-Massuard, M.C., Denevault-Sabourin, C., 2018. Structure-based design of novel quinoxaline-2-carboxylic acids and analogues as Pim-1 inhibitors. Eur. J. Med. Chem. 154, 101–109.

Peng, H., Huang, N., Qi, J., Xie, P., Xu, C., Wang, J., Yang, C., 2003. Identification of novel inhibitors of BCR-ABL tyrosine kinase via virtual screening. Bioorg. Med. Chem. Lett 13, 3693–3699.

Pettersen, E.F., Goddard, T.D., Huang, C.C., Couch, G.S., Greenblatt, D.M., Meng, E.C., Ferrin, T.E., 2004. UCSF Chimera–a visualization system for exploratory research and analysis. J. Comput. Chem. 25, 1605–1612.

Prudencio, M., Hart, P.J., Borchelt, D.R., Andersen, P.M., 2009. Variation in aggregation propensities among ALS-associated variants of SOD1: correlation to human disease. Hum. Mol. Genet. 18, 3217–3226.

Quemener, A., Maillasson, M., Arzel, L., Sicard, B., Vomiandry, R., Mortier, E., Dubreuil, D., Jacques, Y., Lebreton, J., Mathe-Allainmat, M., 2017. Discovery of a small-molecule inhibitor of interleukin 15: pharmacophore-based virtual screening and hit optimization. J. Med. Chem. 60, 6249–6272.

Ramsbeck, D., Hamann, A., Richter, G., Schlenzig, D., Geissler, S., Nykiel, V., Cynis, H., Schilling, S., Buchholz, M., 2018. Structure-guided design, synthesis, and characterization of next-generation meprin beta inhibitors. J. Med. Chem. 61, 4578–4592.

Ray, S.S., Nowak, R.J., Brown Jr., R.H., Lansbury Jr., P.T., 2005. Small-molecule-mediated stabilization of familial amyotrophic lateral sclerosis-linked superoxide dismutase mutants against unfolding and aggregation. Proc. Natl. Acad. Sci. U. S. A. 102, 3639–3644.

Reaume, A.G., Elliott, J.L., Hoffman, E.K., Kowall, N.W., Ferrante, R.J., Siwek, D.F., Wilcox, H.M., Flood, D.G., Beal, M.F., Brown Jr., R.H., Scott, R.W., Snider, W.D., 1996. Motor neurons in Cu/Zn superoxide dismutase-deficient mice develop normally but exhibit enhanced cell death after axonal injury. Nat. Genet. 13, 43–47.

Shvil, N., Banerjee, V., Zoltsman, G., Shani, T., Kahn, J., Abu-Hamad, S., Papo, N., Engel, S., Bernhagen, J., Israelson, A., 2018. MIF inhibits the formation and toxicity of misfolded SOD1 amyloid aggregates: implications for familial ALS. Cell Death Dis. 9, 107.

Tateno, M., Kato, S., Sakurai, T., Nukina, N., Takahashi, R., Araki, T., 2009. Mutant SOD1 impairs axonal transport of choline acetyltransferase and acetylcholine release by sequestering KAP3. Hum. Mol. Genet. 18, 942–955.

Tortorella, P., Laghezza, A., Durante, M., Gomez-Monterrey, I., Bertamino, A., Campiglia, P., Loiodice, F., Daniele, S., Martini, C., Agamennone, M., 2016. An effective virtual screening protocol to identify promising p53-MDM2 inhibitors. J. Chem. Inf. Model. 56, 1216–1227.

Tsuburaya, N., Homma, K., Higuchi, T., Balia, A., Yamakoshi, H., Shibata, N., Nakamura, S., Nakagawa, H., Ikeda, S.I., Umezawa, N., Kato, N., Yokoshima, S., Shibuya, M., Shimonishi, M., Kojima, H., Okabe, T., Nagano, T., Naguro, I., Imamura, K., Inoue, H., Fujisawa, T., Ichijo, H., 2018. A small-molecule inhibitor of SOD1-Derlin-1 interaction ameliorates pathology in an ALS mouse model. Nat. Commun. 9, 2668.

Villa, S., Legnani, L., Colombo, D., Gelain, A., Lammi, C., Bongiorno, D., Ilboudo, D.P., McGee, K.E., Bosch, J., Grazioso, G., 2018. Structure-based drug design, synthesis and biological assays of P. falciparum Atg3-Atg8 protein-protein interaction inhibitors. J. Comput. Aided Mol. Des. 32, 473–486.

Wang, Z., Kang, Y., Li, D., Sun, H., Dong, X., Yao, X., Xu, L., Chang, S., Li, Y., Hou, T., 2018. Benchmark study based on 2P2IDB to gain insights into the discovery of small-molecule PPI inhibitors. J. Phys. Chem. B 122, 2544–2555.

Xu, Y., Yue, L., Wang, Y., Xing, J., Chen, Z., Shi, Z., Liu, R., Liu, Y.C., Luo, X., Jiang, H., Chen, K., Luo, C., Zheng, M., 2016. Discovery of novel inhibitors targeting the menin-mixed lineage leukemia interface using pharmacophore- and docking-based virtual screening. J. Chem. Inf. Model. 56, 1847–1855.

Zhou, H., Zhou, W., Zhou, B., Liu, L., Chern, T.R., Chinnaswamy, K., Lu, J., Bernard, D., Yang, C.Y., Li, S., Wang, M., Stuckey, J., Sun, Y., Wang, S., 2018. High-affinity peptidomimetic inhibitors of the DCN1-UBC12 protein-protein interaction. J. Med. Chem. 61, 1934–1950.